J Mater Sci: Mater Med (2008) 19:3465–3472
DOI 10.1007/s10856-008-3505-3

The anatase phase of nanotopography titania plays an important role on osteoblast cell morphology and proliferation

Jie He · Wei Zhou · Xiaojian Zhou · Xiaoxia Zhong · Xiuli Zhang · Pengbo Wan · Bangshang Zhu · Wantao Chen

Received: 5 January 2008 / Accepted: 16 June 2008 / Published online: 1 July 2008

Abstract The surface properties of biomaterials play a vital role in cell morphology and behaviors such as cell adhesion, migration, proliferation and differentiation. Three different crystal phases of titania film (rutile, anatase and amorphous titania) with similar roughness were successfully synthesized by DC reactive magnetron sputtering. The surface roughness of each film was about 8–10 nm. Primary rat osteoblasts were used to observe changes in morphology and to evaluate cell behavior at the film surface. The number of the osteoblasts on anatase film was significantly higher than rutile and amorphous films after 36 and 72 h incubation. More importantly, synthesis of alkaline phosphatase was significantly greater by osteoblasts cultured on anatase film than on rutile and amorphous films after 7 and 14 days. In addition, the cells grown on the anatase phase film had the largest spreading area; the actin filaments in cells with regular directions were well defined and fully spreaded. The results indicate that the anatase phase of titania with nanoscale topography yield the best biological effects for cell adhesion, spreading, proliferation and differentiation. There are strong therapeutic prospects for this biomaterial film for osteoblast proliferation, with possible applications for orthopedic and dental implant.

J. He and W. Zhou contributed to this work equally.

J. He · X. Zhou · P. Wan · W. Chen (✉)
Department of Oral and Maxillofacial Surgery, Ninth People's Hospital, Shanghai Jiao Tong University School of Medicine, Shanghai 200011, China
e-mail: chenwantao2002@hotmail.com

W. Zhou · X. Zhong
Department of Physics, Shanghai Jiao Tong University, Shanghai 200030, China

X. Zhou · X. Zhang · W. Chen
Shanghai Key Laboratory of Stomatology, Shanghai 200011, China

B. Zhu
Instrumental Analysis Center, Shanghai Jiao Tong University, Shanghai 200030, China

1 Introduction

Titanium is extensively used for biomedical applications, especially for bone-anchoring systems, such as dental, orthopedic implants and osteosynthesis applications [1]. It has excellent bulk mechanical properties such as low modulus of elasticity, high strength-to-weight ratio, and passive surface properties. The excellent corrosion resistance, low rate of ion release, and high degree of biocompatibility of titanium is largely attributed to its inert surface oxide film [2, 3]. However, titanium is bioinert, and a thin connective tissue capsule is likely to surround the material when used as an implant [4]. The efficacy of orthopedic or dental implants requires a mechanically interface with complete osseointegration between the material surface and the bone tissue, with no fibrous tissue interfaces. Thus, the bioactivity of a titanium surface must be improved. Many methods such as chemical vapor deposition (CVD) [5], sol–gel [6], thermal spraying [7], and DC sputtering [8, 9] have been used to prepare bioactive titania coatings.

The physical structure of a biomaterial surface is now known to play a vital role in determining cellular responses. Thus, surface modification is applied to obtain suitable properties for biomedical applications [10, 11]. In recent years, researchers found that the nanoscale features had

significant influences on cell behavior such as morphology, adhesion, migration, proliferation, cytoskeletal organization, differentiation, and apoptosis, both in vitro and in vivo [12–15]. As a result, materials with nanoscale features have been adopted to improve the surface bioactivity and have shown certain success. DC magnetron sputtering is a convenient method to prepare nanoscale titania coatings on a material surface [8]. Many researchers have reported on the biocompatibility of implants in terms of bone cell response and found the effects of titania coatings depend on the surface topography, chemistry, surface energy, and roughness of the biomaterials [16, 17]. However, the role of different crystal phases of the titania on bone cell behavior is still unknown.

In our previous study, the crystal phase of titania had been successfully synthesized by DC reactive magnetron sputtering [9, 18]. In this study, we deposited a different crystal phase of titania film by reactive magnetron sputtering. The surface properties of the films were characterized by atomic force microscopy (AFM), X-ray diffractiometer (XRD), and contact angle goniometer. The primary rat osteoblasts were used to investigate the responses of the cells to the different phases of titania.

2 Material and methods

2.1 Titania coat fabrication

Mirror polished silicon (Si) wafers were used as substrates for deposition of the Titanium oxide (TiO_2) films. Prior to deposition, the substrates were ultrasonically cleaned with ethanol, rinsed with deionized water for 15 min, and dried in air.

The TiO_2 films were fabricated by a reactive DC magnetron sputtering technique according to previously reported methods [18]. The distance between the sputtering target and deposition substrates was 90 mm. The titanium target 99.9% purity (FHR Anlagenbau GmbH, Germany) of 60 mm diameter and 3 mm thickness was mounted on the magnetron cathode. A pumping system was used to achieve a base pressure below 1.0×10^{-4} Pa. High-purity argon (99.999%) and oxygen (99.5%) were used as sputtering and reactive gases, respectively. Three different sets of process conditions were used to synthesize the titania films. Three kinds of specimens were fabricated using the same deposition power of 40 W, the same DC substrate bias of −100, but different total pressures of 0.3, 1.2 and 3.6 Pa, respectively.

2.2 Surface characterization

The surface morphology of the substrates was observed by atomic force microscopy (AFM, Nanoscope®III, USA) with a contact mode. The surface roughness was calculated from the AFM image by image analysis software (Nanoscope®III, USA). Measurements were run in triplicate for each specimens.

The wettability of the deposited TiO_2 film was characterized by water contact angle. Contact angle were measured with deionized H_2O by the sessile drop method, using an optical contact angle-measuring device (OCA20, Dataphysics, Germany). For crystal structure analysis, a thin film X-ray diffractiometer (Rigaku TF-XRD, D/max2550VB/PC, Japan) was used with CuKα radiation, from 10° to 80° (2θ).

2.3 Biocompatibility study

2.3.1 Cell culture

Primary rat osteoblasts (PRO) were obtained using the standard method [19] by sequential enzyme digestion of excised calvarial bones from two-day-old neonatal Sprague-Dawley rats, using a three-step process (1% trypsin in PBS for 10 min; 0.2% collagenase type II in Hanks balanced salt solution (HBSS) for 30 min; 0.2% collagenase type II in HBSS for 60 min). The first two digests were discarded, and the cells were re-suspended in Dulbecco's Modified Essential Medium (Gibco, USA) supplemented with 10% heat-inactivated fetal bovine serum, 2 mmol/l L-glutamine, 100 units/ml penicillin, 100 units/ml streptomycin and amphotericin (complete mixture abbreviated to DMEM). Cells were cultured for 7 days in a humidified atmosphere of 5% CO_2–95% air at 37°C in 25 cm^2 flasks until confluent. Cells were then detached using trypsin/EDTA (0.25% w/v trypsin/0.02% EDTA of pH 7.2). The osteoblastic phenotype of these cells was determined by alkaline phosphatase activity and formation of calcium-containing mineral deposits in the extracellular matrix. Subsequently, cells were re-suspended in the supplemented culture medium as described above, and seeded with the density of 2×10^4 cells/cm^2 on treated specimen surfaces for the biocompatibility study.

2.3.2 Cell attachment, morphology and spreading assay

After 8 h of incubation, cells were fixed for 20 min by 2% glutaraldehyde in 0.01 mol/l PBS. Cells were rinsed in a cacodylate buffered solution, dehydrated in a series of ethanol, and then dried by conventional critical point drying for 2 h. After coated with gold (99.99%), the cell morphology was investigated by SEM (FEI SIRION 200, USA). The number of attached cells was calculated by Image-plus 5.0 software for three random areas from SEM observation field (300×). Cell areas were measured with 50 measurements per sample using NIH Image software for

three random areas from SEM observation field (300×). Measurement value was reported as the mean of cell area.

2.3.3 Cell proliferation

After fixed in 4% paraformaldehyde (Sigma, USA), cells were stained with Acridine Orange (AO, Sigma, USA) and the number of cells was examined with a fluorescent microscope (200×). The number of cells in the observation field was calculated by Image-plus 5.0 software for at least eight random areas at 36 and 72 h for each specimens.

2.3.4 Actin cytoskeleton

Cells were seeded on specimen surfaces for 12 h and rinsed with 0.01 mol/l PBS. The cells were fixed in 4% paraformaldehyde (0.01 mol/l PBS) for 20 min, washed in 0.01 mol/l PBS, permeabilized with 0.1% Triton X-100 in 0.01 mol/l PBS for 4 min, and washed in 0.01 mol/l PBS. To reduce nonspecific background staining with these conjugates, 1% bovine serum albumin was added to the staining solution and the cells were stained by fluorescent rhodamine phalloidin (Invitrogen, USA) for 20 min, then rinsed in 0.01 mol/l PBS. After washed in 0.01 mol/l PBS, the specimens were mounted onto coverslips and sealed with Mounten Media (Invitrogen, USA).

The actin cytoskeleton was examined with a confocal laser-scanning microscope (CLSM, TCS SP2, Leica, Germany) adapted for inverted microscope. The images were taken using a 200× (NA 1.4, oil) Leitz Plan-Apochromatic objective.

2.3.5 Alkaline phosphatase activity

To measure the differentiation of cells on each sample, alkaline phosphatase (ALP) activity test was carried out [20]. After 7 and 14 days incubation periods, the samples were washed by PBS and transferred to a new 6-well polystyrene culture plate. Triton X-100 (500 µl of 0.1%, Sigma,USA) was added to each well. After incubation in 5% CO_2 incubator for 2 h, the solutions were transferred to a micro centrifuge tube and frozen at −80°C for 2 h. After three times freezing–thawing cycles, ALP substrate solution (*p*NPP, Sigma) was added to each solution and the solutions were mixed at room temperature for 30 min, 350 µl of 1 M NaOH was added to stop the reaction. The absorbance of each solution was measured at the wavelength of 405 nm by spectrophotometer. Total protein content was determined with the BAC method in aliquots of the same sample with the PIERCE protein assay kit, read at 562 nm and calculated according to a series of albumin standards. ALP levels were normalized against the total protein content at the end of the experiment. All experiments were conducted in triplicate.

2.4 Statistical analysis

Statistical analysis was made by one-way analysis of variance and adjusted by the Bonferroni method. Differences were considered statistically significant when $P < 0.05$.

3 Results

3.1 Structural characterization

In this study, three kinds of specimens were generated under the same deposition power P = 40 W and negative DC bias on the substrate V = 100 V. In order to obtain different kinds of crystal phase titania, different working pressures (P = 0.3, 1.2 and 3.6 Pa) were utilized, and the specimens were named as T03P, T12P and T36P. The synthetic parameters of each specimen were summarized in Table 1.

X-ray diffraction (XRD) patterns of film synthesized were shown in Fig. 1a. The processing conditions were listed in Table 1. T03P film revealed a wide diffraction peak of Ru (110), which originated from very small rutile nanocrystals. Since there were no other diffraction peaks, the T03P was considered the crystal of pure rutile phase. When the total pressure increased to 1.2 Pa, no diffraction peaks had been detected in T12P film. Thus, the T12P film was either purely amorphous or contained ultra-small nanocrystallites undetectable by XRD. However, the T36P diffraction patterns showed peaks corresponding to An(101), An(103), An(004), An(200), An(211) and An(204) crystalline planes, indicating that the T36P film was composed of anatase titanium dioxide. The three-dimensional surface morphology of the TiO_2 film imaged by the AFM over a surface area of 0.5 × 0.5 µm (Fig. 1b). The processing parameters were shown separately for each of the specimens. The surface roughness was similar for the three kinds of specimens, being approximately 8–10 nm.

The wettability of the films was characterized by the water contact angle. The water contact angles for the TiO_2 films deposited under three processing conditions were shown in Fig. 2a. The water contact angles for the T03P and T12P specimens were the same and near 90° and that of T36P specimen was near 60° (Fig. 2b).

Table 1 Summary of depositon condition of TiO_2 films

Samples	Depositon conditions		
	Pressure (Pa)	Power (W)	Bias
T36P	3.6	40	−100
T12P	1.2	40	−100
T03P	0.3	40	−100

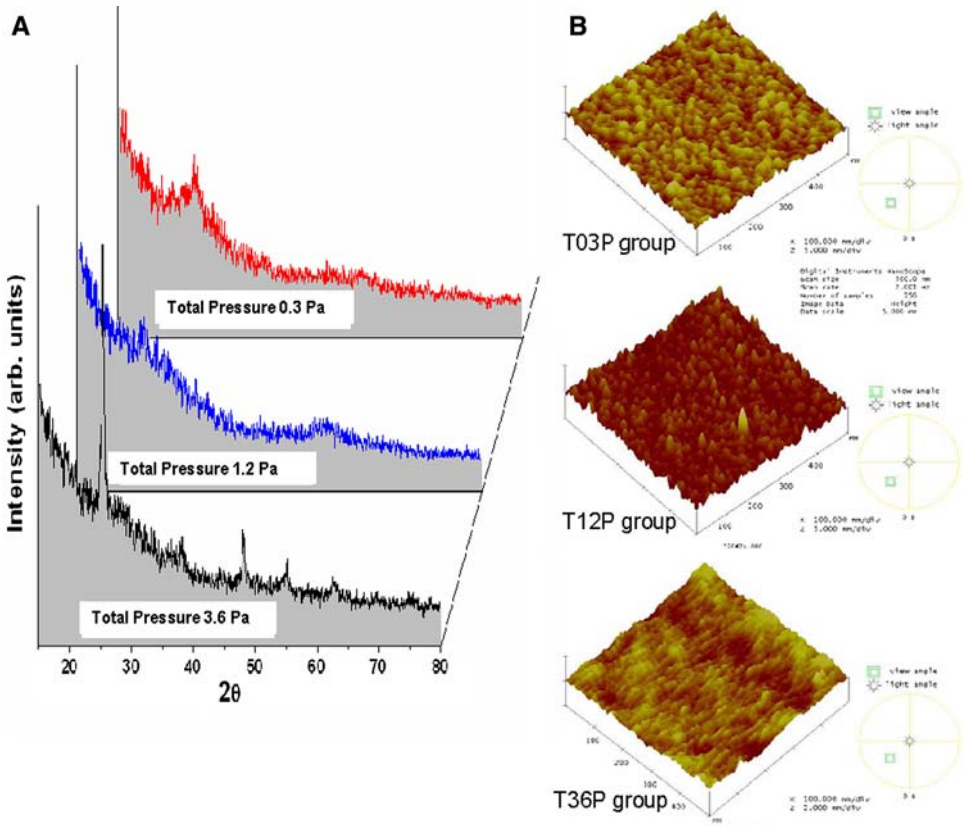

Fig. 1 XRD patterns of the TiO_2 film deposited on films under different conditions. Those shown in (**a**) were analyzed by a thin film X-ray diffractiometer. Three dimensional nanoscale surface morphology of the films was observed by atomic force microscopy (**b**)

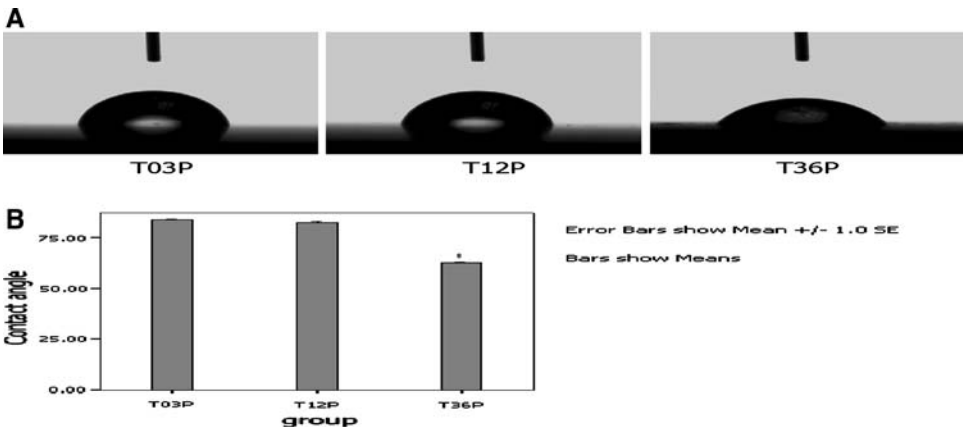

Fig. 2 The water contact angle of different samples (**a**) and the histogram of the water contact angle of different films (**b**) were examined by the water contact angle method.* represented significant differences between marked group with the other two groups

3.2 Morphological analyses, attachment and spreading area assay

PRO cells grown on T03P, T12P and T36P sample surfaces exhibited intact, well-defined morphology. SEM analysis showed the differences in cell morphology (Fig. 3). Morphological features were assessed in terms of cell attachment, cell adhesion, and spreading on the substratum. The cells had three typical morphological features: (1) rounded and hemispheroidal with filipodium (Fig. 3a); (2) flat with a lamellipodium (Fig. 3b); (3) flat morphology with cytoplasmic extensions (Fig. 3c).

The results showed that the nanophase TiO_2 film synthesized by DC magnetron sputtering deposition significantly promoted osteoblast adhesion and spreading. The T36P had a better influence on osteoblast adhesion and spreading than T03P and T12P. Most cells in the T36P group (Fig. 3f) were flat and spread out with projecting cytoplasmic extensions, while most cells in the T03P group (Fig. 3d) and T12P group (Fig. 3e) were hemispheroidal with filopodium and flat with lamellipodium. The cell attachment was also confirmed by the cell number counting after 8 h incubation (Fig. 3d–f). The results showed that the number of attached cells in T36P group was higher

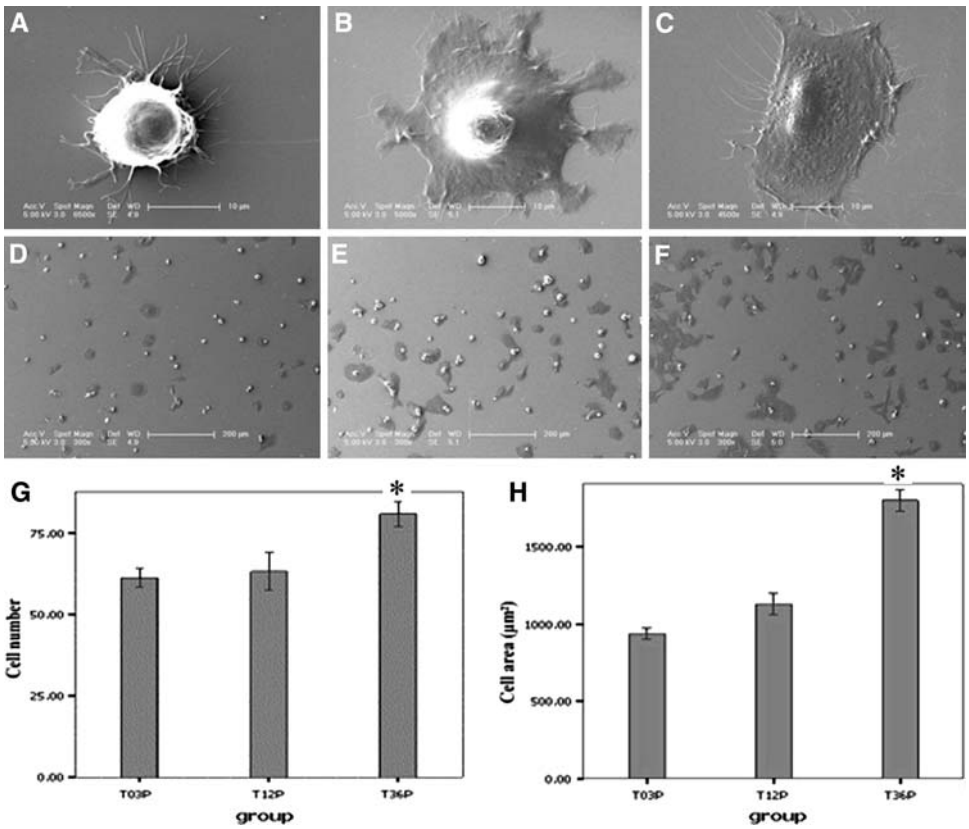

Fig. 3 Scanning electron micrographs demonstrated the morphology of primary rat osteoblast after 8 h of incubation. There were three typical morphological features: rounded and hemispheroidal with filipodium (**a**, magnification was 6500); flat with a lamellipodium (**b**, magnification was 5500); flat morphology with cytoplasmic extensions (**c**, magnification was 4500). Most cells in the T36P group were flat and spread (**f**), while most cells in the T03P (**d**) and T12P (**e**) groups were hemispheroidal and flat with a lamellipodium. The number of attached cells after 8 h incubation was shown in (**g**). Cells on T36P group was higher ($P < 0.05$) than other group specimens. There was no statistically significant difference between the T03P and T12P groups. Cell areas for 50 cells from random fields (ESM, magnification was 300) were measured using NIH Image Software and were recorded as the mean cell area (μm^2). Each point represents the average of triplicate experiments. The cell area in T36P group was higher ($P < 0.05$) than the other two groups (**h**). * represented significant differences between marked group with the other two groups

($P < 0.05$) than the other two specimens and there was no significant difference between the T03P and T12P groups (Fig. 3g, $P > 0.05$). The spreading cell area was measured using NIH Image software at 8 h culture. The average of cell area on these films was shown in Fig. 3h. The cell area in T36P group was higher than the other two groups ($P < 0.05$) and there was no significant difference between T03P and T12P groups ($P > 0.05$).

3.3 Proliferation of cells

Cell growth in different specimens and a histogram of cell numbers after 36 and 72 h incubations were shown in Fig. 4a and b. All three types of specimen surfaces were able to support cell growth as the metabolic activity of PRO cells increased with the incubation time less than 36 h. However, significant differences were found at 36 h between the T03P and T36P group. Cell number in the T36P group was higher than other groups ($P < 0.05$) and there was no significant difference between the T03P and T12P groups ($P > 0.05$). After 72 h incubation, the number of cells in the T36P group was still higher than the other two groups ($P < 0.05$).

3.4 Cytoskeleton

Confocal microscope images of the cytoskeleton, stained by Rhodamine-phalloidin after 12 h incubation were shown in Fig. 5. In all three types of specimens, cells maintained their typical morphology. The cellular morphology was different in different groups. Numerous well-defined actin filaments were observed in T03P (Fig. 5a) and T12P groups (Fig. 5b), and interestingly, actin filaments extended in irregular directions in both groups. The actin filament distribution was fully spread in T36P group (Fig. 5c). Moreover, all of the actin filaments with regular directions in T36P group were well-defined and the actin microfilament system ran parallel to the long axis of the

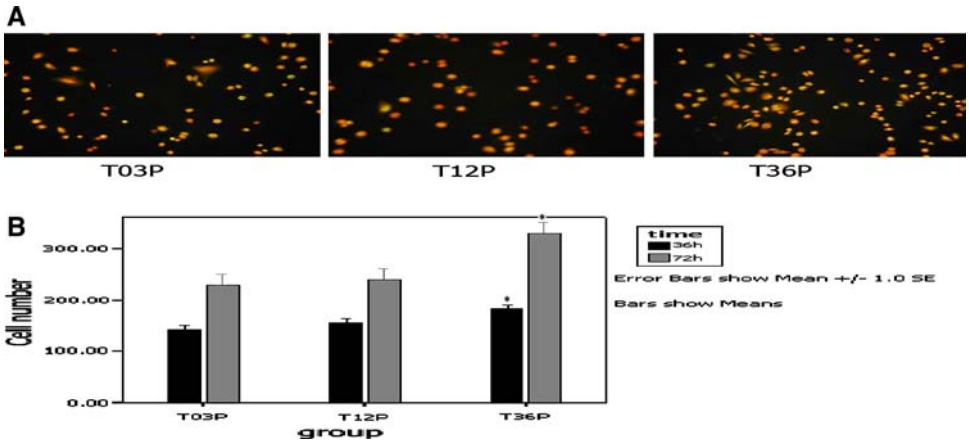

Fig. 4 Fluorescence microscope image of primary rat osteoblasts cultured for 36 h on different specimen surfaces (**a**). Cells were stained by AO fluorescent dye. Cell proliferation of primary rat osteoblasts cultured on different group surfaces was shown. The initial seeding density was 2×10^4 cell/cm^2. A significant difference was found for the T36P group compared to others in 36 and 72 h after incubation; the number of cells in T36P group was higher than others (**b**). * represented significant differences between marked group with the other two groups

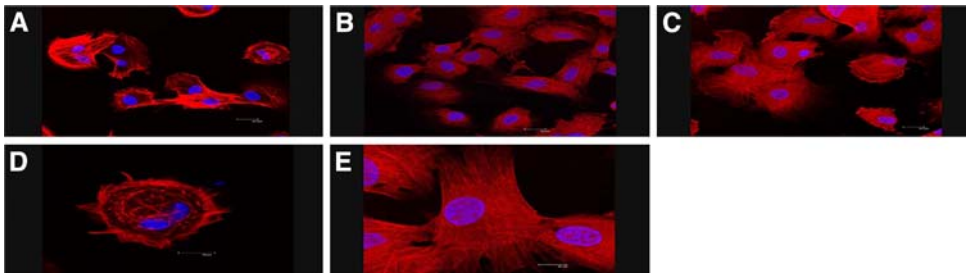

Fig. 5 The changes in the actin cytoskeleton of primary rat osteoblasts after 12 h incubation were shown in T03P (**a**), T12P (**b**), T36P (**c**); the high magnification images showing the direction of the actin microfilament system were shown in the T03P group (**d**) and the T36P group (**e**), which were stained by fluorescent rhodamine phalloidin and observed by confocal fluorescence microscope

cells (Fig. 5e) while it ran in irregular directions in the other two groups (Fig. 5d).

3.5 Alkaline phosphatase activity

The ALP activity of PRO increased gradually with the extension of incubation time. Cells in T36P group presented higher activity of ALP than the other two groups at 7th and 14th day (Fig. 6, $P < 0.05$). However, there were no significant differences between T03P and T12P groups.

4 Discussion

The purpose of this study is to investigate which crystal phase of titania film among three with similar nanotopography will favor osteoblast adhesion, spreading, proliferation and differentation. In the course of cell–material interaction, protein adsorption is one of the first occurrences at the solid/liquid interface [17, 21]. It has been reported that the surface topography of a substrate can affect the expression of

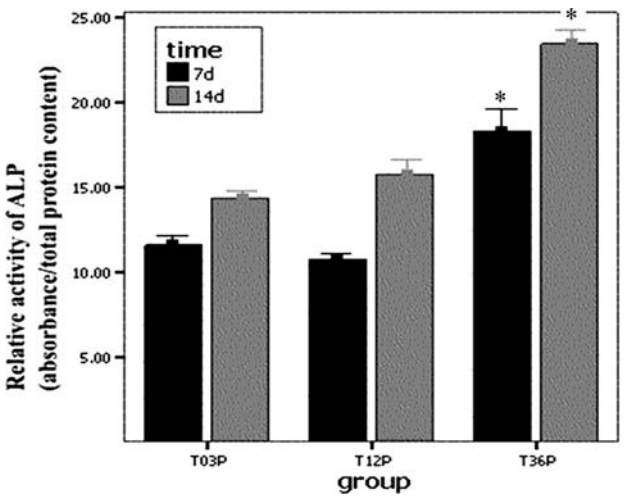

Fig. 6 The ALP activity of primary rat osteoblasts on samples was measured with the *p*NPP assay and normalized on the basis of protein content per disk. Cells in T36P group presented higher activity than the other two groups ($P < 0.05$) at 7th and 14th day. There was no significant difference between T03P and T12P groups. * represented significant differences between marked group with the other two groups

fibronectin and vitronectin integrin receptors [12, 22], and can modify their clustering or aggregation, therefore determining variations in the shape and spreading of cells. During the process of cell spreading, the shape of cells is changed and the cellular skeleton is reorganized. In our experiments, the shapes of cells on different specimen surfaces were very distinct. This might be attributed to the effects of nanotopography. In native tissues, nanoscale protein interactions are crucial for regulating cell functions such as proliferation, migration, and ECM production [17, 23, 24]. Protein adsorption depends on the surface features of the implanted biomaterials such as roughness, chemistry and wettability. The particle size of the biomaterial influences these surface properties and the corresponding protein interactions [20, 25, 26]. Recent reports have demonstrated that the nanoscale biomaterials have special properties to improve interactions between material and proteins that regulate cellular function [25–27]. Some studies reported a fully spreading flattened cell morphology and a regular cytoskeleton was "better" with respect to biocompatibility [28, 29]. For the above mentioned reason, the cells on these specimen surfaces appear more flat and spreading out, resulting in a larger cell spreading area, especially in T36P group after 8 h incubation. Since spreading is an essential step in cell adhesion, prior to an exponential growth phase, cell spreading can have a profound effect on cell proliferation and differentiation. In our experiments, cell proliferation and differentiation were also enhanced by the nanostructure surfaces, which resulted in a more rapid and distinct polygonal spreading of the cells. Our study also revealed that cell adhesion and proliferation were remarkably enhanced by the nanotopography of the titania coating deposited by DC magnetron sputtering than by a no-nanotopography TiO2 layer on a titanium surface (data is not presented here).

Comparisons of the cell adhesion, spreading, proliferation and differentiation between T03P and T12P groups reveal no statistical difference, but there are significantly different from T36P. Cells showed better adhesion, spreading, proliferation and differentiation when cultured on T36P substrates. Although cell adhesion and proliferation can also be affected by surface chemistry, wettability, or other factors, many studies have demonstrated that nanoscale surface topography plays a vital role in regulating osteoblast responses [20, 23, 25]. In this study, the composition of the three kinds of film is titania, which means that the chemistry of all the films are the same. Furthermore, the roughness of the three specimens are also similar. Cai et al. have shown that the surface roughness has little effect on protein adsorption and cell growth behavior [30, 31]. The different phases of titania have different physicochemical properties and surface wettability is an important physicochemical property that could regulate cell behavior; many studies have been performed to assess the effects of surface wettability on cell behavior using different methods [32]. Most studies indicate that cells tend to attach onto hydrophilic surfaces rather than hydrophobic surfaces [32, 33], which is consistent with our experiment. The hydrophilic surface could favor cell adhesion and thus improve proliferation and differentiation without changing surface morphology and chemistry. Therefore, the T36P specimen, with a more hydrophilic surface compared to T03P and T12P specimens, enhances cell adhesion, spreading, proliferation and differentiation. Moreover, the anatase phase of titania exhibited better biocompatibility in comparison with the amorphous rutile phase, mainly due to surface wettability.

5 Conclusions

Our findings indicate that cell spreading, adhesion, proliferation and differentiation of PRO cells are influenced both by the topography of the surface and the phase of titania. Osteoblasts spread and grow well on the nanoscale topography surface mainly due to their nanotopography; the anatase phase of titania film enhances osteoblast adhesion, proliferation and differentiation by affecting surface contact angles and/or wettability. This study has demonstrated that the anatase phase with nanotopography might be a promising method for the surface modification of dental and orthopedic implants.

Acknowledgements The authors would like to thank Mrs. QH Lu (Analysis and Measurement Center of Shanghai JiaoTong University) for AFM measurement and modification of the manuscript. The project was financially supported by the National Natural Science Foundation of China (30572053) and Shanghai Science and Technology Committee (0452nm063 and 0652nm018).

References

1. K. Bordji, J.Y. Jouzeau, D. Mainard et al., Biomaterials **17**, 929 (1996). doi:10.1016/0142-9612(96)83289-3
2. Black J, Hasting G, in *Handbook of Biomaterial Properties*. (Chapman & Hall, London, 1998), p. 179
3. S.H. Oh, R.R. Finones, C. Daraio et al., Biomaterials **26**, 4938 (2005). doi:10.1016/j.biomaterials.2005.01.048
4. M. Karlsson, E. Palsgard, P.R. Wilshaw et al., Biomaterials **24**, 3039 (2003). doi:10.1016/S0142-9612(03)00146-7
5. D.A. Boyd, L. Greengard, M. Brongersma et al., Nano. Lett. **11**, 2592 (2006). doi:10.1021/nl062061m
6. X. Chen, S.S. Mao, J. Nanosci. Nanotechnol. **4**, 906 (2006). doi:10.1166/jnn.2006.160
7. S. Leeuwenburgh, J. Wolke, J. Schoonman et al., J. Biomed. Mater. Res. A **74**, 275 (2005). doi:10.1002/jbm.a.30420
8. R. Rabady, I. Avrutsky, Appl. Opt. **44**, 378 (2005). doi:10.1364/AO.44.000378
9. W. Zhou, X. Zhong, X. Wu et al., J. Biomed. Mater. Res. A **81**, 453 (2007). doi:10.1002/jbm.a.30987
10. O. Suzuki, S. Kamakura, T. Katagiri, J. Biomed. Mater. Res. B Appl. Biomater. **77**, 201 (2006). doi:10.1002/jbm.b.30407

11. C.J. Wilson, R.E. Clegg, D.I. Leavesley et al., Tissue Eng. **11**, 1 (2005). doi:10.1089/ten.2005.11.1
12. R. Kriparamanan, P. Aswath, A. Zhou et al., J. Nanosci. Nanotechnol. **6**, 1905 (2006)
13. M. Sato, T.J. Webster, Expert Rev. Med. Devices **1**, 105 (2004). doi:10.1586/17434440.1.1.105
14. C. Yao, T.J. Webster, J. Nanosci. Nanotechnol. **6**, 2682 (2006). doi:10.1166/jnn.2006.447
15. T.J. Webster, E.S. Ahn, Adv. Biochem. Eng. Biotechnol. **103**, 275 (2007)
16. A.F. Von Recum, T.G. Van kooten, J. Biomater. Sci. Polym. Ed. **7**, 181 (1995). doi:10.1163/156856295X00698
17. K. Anselme, Biomaterials **21**, 667 (2000). doi:10.1016/S0142-9612(99)00242-2
18. W. Zhou, X. Zhong, X. Wu et al., Surf. Coat. Technol. **200**, 6155 (2006). doi:10.1016/j.surfcoat.2005.09.029
19. T. Lee, S. Tsai, E. Chang et al., J. Mater. Sci. Mater. Med. **13**, 281 (2002). doi:10.1023/A:1014010901423
20. T.J. Webster, C. Ergun, R.H. Doremus, Biomaterials **21**, 1803 (2000). doi:10.1016/S0142-9612(00)00075-2
21. K. Anselme, M. Bigerelle, Biomaterials **27**, 1187 (2006). doi:10.1016/j.biomaterials.2005.10.009
22. D.M. Brunette, B. Chehroudi, J. Biomech. Eng. **121**, 49 (1999). doi:10.1115/1.2798042
23. E.K. Yim, K.W. Leong, Nanomedicine **1**, 10 (2005)
24. E. Eisenbarth, D. Velten, J. Breme, Biomol. Eng. **24**, 27 (2007). doi:10.1016/j.bioeng.2006.05.016
25. V. Perla, T.J. Webster, J. Biomed. Mater. Res. A **75**, 356 (2005). doi:10.1002/jbm.a.30423
26. M. Sato, E.B. Slamovich, T.J. Webster, Biomaterials **26**, 1349 (2005). doi:10.1016/j.biomaterials.2004.04.044
27. T.J. Webster, J.U. Ejiofor, Biomaterials **25**, 4731 (2004). doi:10.1016/j.biomaterials.2003.12.002
28. B.S. Zhu, Q.Q. Zhang, Q.H. Lu, Biomaterials **25**, 4215 (2004). doi:10.1016/j.biomaterials.2003.11.020
29. B. Zhu, Q. Lu, J. Yin et al., Tissue Eng. **11**, 825 (2005). doi:10.1089/ten.2005.11.825
30. K. Cai, J. Bossert, K.D. Jandt, Colloids Surf. B Biointerfaces **49**, 136 (2006). doi:10.1016/j.colsurfb.2006.02.016
31. K. Cai, A. Rechtenbach, J. Hao et al., Biomaterials **26**, 5960 (2005). doi:10.1016/j.biomaterials.2005.03.020
32. Y. Arima, H. Iwata, Biomaterials **28**, 3074 (2007). doi:10.1016/j.biomaterials.2007.03.013
33. J. Wei, M. Yoshinari, S. Takemoto et al., J. Biomed. Mater. Res. B Appl. Biomater **81**, 66 (2007). doi:10.1002/jbm.b.30638